The SF3b155 N-Terminal Domain Is a Scaffold Important for Splicing[†]

Danielle M. Cass and J. Andrew Berglund*

Department of Chemistry and Institute of Molecular Biology, University of Oregon, Eugene, Oregon 97403

Received March 3, 2006; Revised Manuscript Received June 9, 2006

ABSTRACT: Recruitment of U2 snRNP to the branch point sequence of introns is a necessary step in pre-mRNA splicing. In the current model, U2AF65, bound at the polypyrimidine tract of the intron, recruits U2 snRNP to the branch point sequence by interacting with the U2 snRNP protein SF3b155. We demonstrate that the N-terminal domain of SF3b155 contains multiple U2AF65 binding sites that are distinct from the binding site for the U2 snRNP protein p14, mapped to amino acids 396−424 of SF3b155. The N-terminal domain of SF3b155 appears to adopt a primarily unfolded structure but is functional to inhibit splicing in vitro. RNA binding studies show that the N-terminal domain of SF3b155 binds RNA nonspecifically and that the sites for U2AF65 binding and RNA binding are overlapping (or the same) within SF3b155. We propose that the N-terminal domain of SF3b155 adopts a primarily unfolded structure that functions as a scaffold to facilitate SF3b155's multiple protein−protein and protein−RNA interactions. The multiple U2AF65 binding sites on SF3b155 suggest a model in which multiple U2AF65 molecules bound to the intron could enhance U2 snRNP recruitment to the branch point sequence.

The removal of nuclear pre-mRNA introns is catalyzed by the spliceosome, a large multisubunit complex composed of small nuclear RNAs (snRNAs)[1] and approximately 100 proteins (reviewed in ref *1*). Three intronic elements are necessary for the two transesterification reactions of splicing: the 5′ splice site (5′SS), the branch point sequence (BPS), and the 3′ splice site (3′SS). A fourth element, the polypyrimidine tract (PyT), located between the BPS and the 3′SS, enhances the recognition and splicing of introns by the spliceosome (*2*−*7*). The branch site adenosine of the BPS is the nucleophile in the first transesterification reaction, releasing the 5′ exon. In the second transesterification reaction the 3′OH of the 5′ exon attacks at the 3′SS, creating the mRNA product. The intronic elements are recognized multiple times by both proteins and/or snRNAs to improve fidelity before the first transesterification reaction (reviewed in ref *8*).

The initial intron recognition complex (E complex) consists of U1 snRNP bound at the 5′SS and SF1, U2AF65, and U2AF35 bound at the BPS, the PyT, and the 3′SS, respectively (*9*−*12*). The latter three proteins bind the 3′ end of introns in a cooperative manner (*10*, *13*). During ATP-dependent A complex formation, U2 snRNP replaces SF1 and U2 snRNA base pairs with the BPS (*14*). However, this base-pairing event is not sufficient to recruit and stabilize U2 snRNP; other factors are required (*15*). U2 snRNP is proposed to be recruited to the BPS primarily through an interaction between the third RNA recognition motif (RRM3) of U2AF65 and SF3b155 (also known as SAP155), a component of U2 snRNP (*16*).

SF3b155 is a highly conserved protein found in both the major and minor spliceosomes. It is part of SF3b, a 450 kDa complex that, along with SF3a and the 12S U2 snRNP, forms the functional 17S U2 snRNP (*17*, *18*). SF3b155 is composed of two regions: the *N*-terminal *d*omain (SF3b155 NTD, amino acids 1−430) and the C-terminus (amino acids 431−1304). The C-terminus of SF3b155 is highly conserved (75% identity between *Schizosaccharomyces pombe* and *Homo sapiens*) and consists of HEAT-like repeats. These repeats wrap around the U2 snRNP and are thought to stabilize the structure of the U2 snRNP (*19*). SF3b155 NTD is less conserved than the C-terminal region, but SF3b155 NTD contains the binding sites for splicing associated factors U2AF65, p14, cyclin E, and Nipp 1 (*16*, *20*−*22*). U2AF35 also interacts with SF3b155 (*16*), but the region of interaction has not been mapped.

In addition to its role in U2 snRNP recruitment, SF3b155 has been proposed to position p14, another U2 and U12 snRNP protein, at the branch point adenosine (*20*). p14 contains an RRM, but binding studies with purified p14 have not shown any specific interaction with the BPS (*20*). However, p14 binds SF3b155, and SF3b155 cross-links to RNA both 5′ and 3′ of the BPS but not at the BPS (*16*, *20*). This information, along with the cryo-EM structure of SF3b placing p14 in the center of the complex, suggests that SF3b155 binding to either side of the BPS facilitates the placement of p14 at the BPS (*19*, *20*, *23*).

Two additional proteins that interact with SF3b155, cyclin E and NIPP1, are proposed to regulate the phosphorylation of SF3b155, which is an important control step that is necessary for the second transesterification reaction of splicing (*24*). Cyclin E−cdk2 phosphorylates SF3b155 NTD

[†] This work was supported by a NSF GK-12 Fellowship (DGE 0231997) to D.M.C. and a grant from the American Heart Association (0560052Z) to J.A.B.

* To whom correspondence should be addressed. Telephone: (541) 346-5097. Fax: (541) 346-5891. E-mail: aberglund@molbio.uoregon.edu.

[1] Abbreviations: 5′SS, 5′ splice site; 3′SS, 3′ splice site; PyT, polypyrimidine tract; snRNA, small nuclear RNA; snRNP, small nuclear ribonuclear protein; SF3b155 NTD, SF3b155 N-terminal domain; RRM, RNA recognition motif; BPS, branch point sequence.

10.1021/bi060429o CCC: $33.50
Published on Web 08/01/2006

in vitro and does so through a specific interaction between SF3b155 NTD and cyclin E (*21*). The dephosphorylation and recycling of SF3b155 are proposed to be mediated by NIPP1, which interacts with SF3b155 NTD and recruits the protein phosphatase PP1 (*22*).

In this study we use biophysical and biochemical assays to investigate many of the interactions that SF3b155 NTD makes during splicing. We show that SF3b155 NTD is an elongated, partially unstructured molecule. This structural elasticity may be important for the many interactions SF3b155 NTD participates in during spliceosome assembly and catalysis. We show that SF3b155 NTD is capable of nonspecifically binding RNA and that the third RRM domain of U2AF65 inhibits this activity. Deletion mapping experiments of SF3b155 NTD identify multiple binding sites for U2AF65 and one p14 binding site. We propose a model in which the multiple interactions of SF3b155's NTD are involved in the recruitment and binding of U2 snRNP at the BPS.

EXPERIMENTAL PROCEDURES

Cloning and Protein Purification. All fragments of SF3b155 were inserted into the pGEX6P-1 plasmid (Amersham) after standard PCR amplification and restriction digestion with *Bam*HI and *Eco*RI. SF3b155 NTD (amino acids 1−430) was amplified from a full-length SF3b155 clone courtesy of Robin Reed. All subsequent constructs (1−360, 1−255, 361−424, 376−424, 396−424, Pep A, Pep C, Pep E, Pep G, Pep H) were amplified from the SF3b155 NTD plasmid. SF3b155 (396−424 W−A) mutation was introduced using QuikChange, following the recommendations from Stratagene. Pep A Mut and Pep G Mut were generated with PCR using the following overlapping DNA primers: Pep A MutF, 5′-CGC GGA TCC GCA GCG TCC CAG CCT CCA TCA AAA CGA AAA CGG CGT GCG GAT CAA ACA G-3′; Pep A MutR, 5′-CCG GAA TTC TTA GGG AGT GGC ACC AGG AGT CTG ATC AGC TGT TTG ATC CGC ACG CC-3′; Pep G MutF, 5′-CGC GGA TCC ACA CCG ACT CCT GGA GCC AGT AAA AGA AAA TCA CGG GCG GAT GAA ACA CC-3′; Pep G MutR, 5′-CCG GAA TTC TTA AGT GCT TCC ACC CAT CTG ACT AGC TGG TGT TTC ATC CGC CCG TG-3′. All clones were confirmed by sequencing.

All SF3b155 constructs were expressed in *Escherichia coli* BL21 cells (Novagen) and grown in 2X-YT media. Cells were induced with 0.25 mM IPTG for 3 h at 37 °C. Cells were then pelleted and frozen at −80 °C overnight. Cells were resuspended in lysis buffer (25 mM Tris, pH 7.5, 300 mM NaCl, 1 mM EDTA, and 2 mM DTT), sonicated, and spun at 19 800*g* for 30 min, and the supernatant was bound to glutathione−agarose beads (Sigma). The GST tag was cleaved with PreScission protease (Amersham) overnight at 4 °C, and SF3b155 was eluted off the beads and bound to a Source 15Q anion-exchange column (Amersham). The protein was eluted from the column over a salt gradient, and the peak fractions were collected, concentrated, and dialyzed in dialysis buffer (150 mM NaCl, 10 mM Tris, pH 7.5, 1 mM EDTA, and 2 mM DTT). The GST-tagged constructs used in the pull-down assays were eluted from the glutathione beads with reduced glutathione and dialyzed into dialysis buffer.

U2AF65 purification was done as described in Henscheid et al. (*25*). U2AF65ΔRRM3 was purified as described previously (*10*). RRM3 of U2AF65 (amino acids 369−474) was cloned into pGEX6P-1 using *Bam*HI and *Eco*RI restriction sites. The RRM3 construct was expressed in *E. coli* BL21 cells and purified in the same manner as the SF3b155 NTD.

Full-length p14 was cloned into pKKT7E (initial clone courtesy of Charles Query) and expressed in *E. coli* BL21, and cells were lysed as above. The p14 extract was bound to a Source 15S cation-exchange column (Amersham) in S buffer A (10 mM MES, pH 6.5, 100 mM NaCl, 1 mM EDTA, and 2 mM DTT) and eluted over a salt gradient. The peak fractions were collected, concentrated, and dialyzed into dialysis buffer. The GST−p14 (10−95) fragment was amplified from the PKKT7E-p14 DNA clone using primers that introduced *Eco*RI and *Xho*I restriction sites and cloned into the pGEX6P-1 vector. GST−p14 was purified as described above for GST−SF3b155.

Analytical Ultracentrifugation. Sedimentation velocity analytical ultracentrifugation experiments were performed using a Beckman XL-1 analytical ultracentrifuge. The experiments were done in 300 mM NaCl, 1 mM EDTA, 1 mM DTT, and 10 mM MES, pH 6.5. The centrifuge was spun at 55 000 rpm for 8 h at 20 °C. Data were collected at 280 nm and analyzed using SEDFIT 85 (*26*).

Gel Filtration Chromatography. A Superdex 200 10/300 GL (Amersham) gel filtration column was used. The column was calibrated using the Amersham LMW and HMW calibration kit, according to the manufacturer's directions. SF3b155 NTD was dialyzed and run in 300 mM NaCl, 1 mM EDTA, 1 mM DTT, and 10 mM MES, pH 6.5, at a flow rate of 0.3 mL/min. Elution from the column was monitored at 280 and 260 nm. The apparent molecular mass was calculated from the linear calibration line.

Circular Dichroism (CD). SF3b155 NTD and U2AF65 were dialyzed into CD buffer (300 mM NaCl and 20 mM KPO_4, pH 7.5). CD was done using a Jasco J-720 sprectropolarimeter from 340 to 195 nm. Samples were measured at 4 °C using a 0.1 cm path length cell at a protein concentration of 0.4 mg/mL. Melting temperature CD of 0.04 mg/mL SF3b155 NTD was done in a 1 cm path length cell at 222 nm over a temperature gradient of 0−89 °C.

RNA Labeling. RNA oligos were ordered from Dharmacon and deprotected according to manufacturer's instructions. AV RNA sequence is 5′-UUCGUGCUGACCCUGUCCCUUUUUUUUCCACAGC-3′. They were then radiolabeled with [γ-^{32}P]ATP, gel purified on a 10% denaturing polyacrylamide gel, and further purified using a Bio-Spin 6 column (Bio-Rad).

Gel Shift Assay. Proteins in dialysis buffer were incubated for 15 min with 0.3 nM RNA in binding buffer (100 mM NaCl, 5 mM $MgCl_2$, 50 mM Tris, pH 7.5, 0.01% Triton X-100, 1 mM DTT, 0.5× TB, 4% glycerol, 0.05% bromophenol blue, and 0.1 mg/mL yeast tRNA). The final volume of the reaction was 10 μL, and 5 μL was loaded onto a native polyacrylamide gel (5% 37.5:1 monoacrylamide:bisacrylamide, 1% glycerol, and 0.5× TB). Gels were run at ∼100 V for 4 h at 4 °C. Gels were dried and exposed using a Phosphoimager screen (Molecular Dynamics) overnight at room temperature. Quantitation of the gels was done using ImagQuant software (Molecular Dynamics). Dissociation

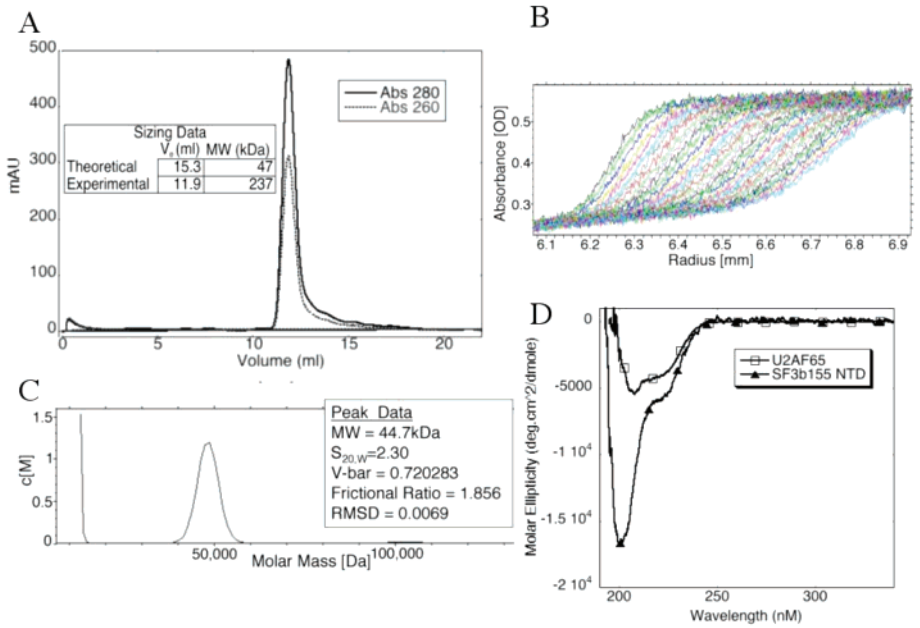

FIGURE 1: SF3b155 NTD is elongated and monomeric in solution. (A) Analytical gel filtration of 10 μM SF3b155 NTD. Protein elution was monitored by absorbance at 280 and 260 nm. The scale on the *X*-axis is the volume after injection onto the column. The inset shows the theoretical elution volume (V_e) for a 47 kDa protein based on a standard curve and the actual V_e for SF3b155 NTD. The molecular mass for the actual V_e is also based on the standard curve. (B, C) Analytical ultracentrifugation results for 20 μM SF3b155 NTD. (B) Sedimentation velocity scans of SF3b155 NTD. Absorbance was scanned at 280 nm, and the distribution of absorbencies is shown as a function of radius. (C) Analysis of the velocity scans using SEDFIT 85. The graph shows the distribution of material with a molecular mass in daltons (Da). (D) CD spectrum of SF3b155 NTD (triangles) compared to U2AF65 (squares). The spectra were taken at 4 °C from 340 to 195 nm.

constants (K_d) were calculated using a one-site binding model, where the fraction bound (Y) = [protein-bound RNA]/[total RNA] is plotted on the *Y*-axis versus the total protein added. To put the fraction bound in terms of total protein, total RNA, and K_d, the following equation was used: [protein-bound RNA] = ([total protein] + [total RNA] + K_d + {(−[total protein] − [total RNA] − K_d)^2 − 4[total protein][total RNA]}$^{1/2}$)/2. The equation for fraction bound was then fit to the data using Kaleidagraph (Synergy Software).

GST Pull-Down Assay. The GST fusion proteins were incubated with non-GST fused protein and glutathione-uniflow resin (BD Biosciences) for 1 h, rotating at 4 °C. Each sample was then washed three times with wash buffer (80−300 mM NaCl, 20 mM Tris, pH 7.5, 0.05% NP-40, 1 mM EDTA, and 1 mM DTT). Bound proteins were eluted in protein denaturing dye, heated for 5 min at 98 °C, run on SDS−PAGE gels, and visualized with Coomassie stain.

Western Analysis. SDS−PAGE gels from the GST pull-down assay were transferred for 1 h at 100 V with a wet transfer system onto nitrocellulose in transfer buffer (25 mM Tris, pH 7.5, 200 mM glycine, and 20% methanol). The membrane was incubated for 1 h with anti-U2AF65 antibody (Santa Cruz Biotechnology), washed three times with TBST (50 mM Tris, pH 7.5, 150 mM NaCl, and 0.1% Tween-20), and incubated with secondary donkey anti-goat Ig-HRP antibody (Santa Cruz Biotechnology). Detection was with chemiluminescence of horseradish peroxidase.

In Vitro Splicing Assay. Splicing assays were done as described previously (*27*). Each splicing reaction contained 20 fmol of AdML pre-mRNA (plasmid courtesy of Robin Reed). Pre-mRNA was made by body labeling with p32−CTP during in vitro transcription along with a methylated guanidine cap. Splicing reactions were incubated for 2 h at 30 °C. Splicing was analyzed by running the reactions on a 15% denaturing polyacrylamide gel for 5−6 h at 1500 V and then exposing the gel overnight to a Phosphoimager screen (Molecular Dynamics).

RESULTS

SF3b155 NTD Is Elongated and Is Unstructured. SF3b155 NTD contains no characterized domains, and secondary structure prediction algorithms suggest it to be natively unstructured (*28*−*30*). High-resolution structures are not available for SF3b155. The cryo-EM structure of the SF3b complex places only the C-terminal HEAT repeats of SF3b155 in the context of the SF3b particle and provides no model for SF3b155 NTD (*19*). Using multiple techniques, we have confirmed that SF3b155 NTD contains limited structure and appears to be an elongated molecule. Gel filtration chromatography shows that SF3b155 NTD elutes at an apparent molecular mass of ∼237 kDa (Figure 1A), whereas its predicted molecular mass is 47 kDa (*31*). GST pull-down experiments do not detect an interaction between SF3b155 NTD and itself (data not shown), suggesting that the aberrant elution of SF3b155 NTD during gel filtration is due to it adopting a nonglobular shape. This possibility is supported by the results of velocity analytical ultracentrifugation (AUC) (Figure 1B), which indicate that SF3b155 NTD is a monomeric, nonspherical molecule. The AUC analysis shows that 87% of the species in solution are distributed in a peak with a sedimentation coefficient ($s_{20,w}$) of 2.30 and a frictional ratio of 1.856 (Figure 1C). The sedimentation coefficient and frictional ratio predict an apparent molecular mass of 44.7 kDa. This is in agreement with the calculated molecular mass of 47 kDa for SF3b155 NTD. The frictional ratio of 1.856 is indicative of an extended, nonsymmetrical shape, in contrast to a globular protein that has a frictional

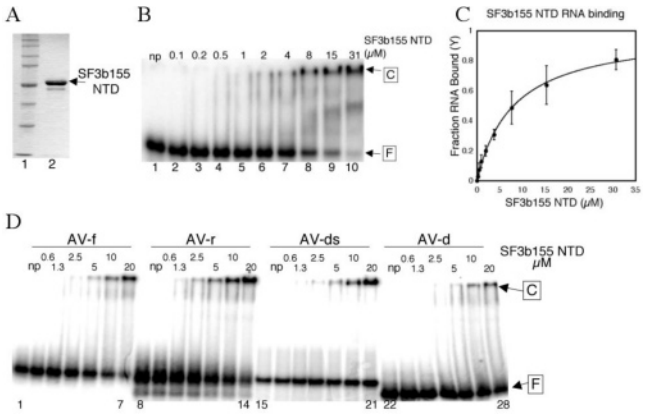

FIGURE 2: SF3b155 NTD binds RNA nonspecifically. (A) Purified SF3b155 NTD at 20 μM run on a 10% SDS gel and stained with Coomassie. (B) The gel shift assay was done with P^{32}-labeled AV RNA. SF3b155 NTD was titrated at the indicated concentrations, while the RNA was held at a constant concentration of 3 nM. C = RNA bound to SF3b155 NTD, F = free RNA, and np = no protein. (C) Quantitation of the gel shift assay was done by graphing the fraction of RNA in complex with SF3b155 NTD [$Y = C/(F + C)$] as a function of SF3b155 NTD concentration. The average of three experiments was graphed (dots) and fitted to a hyperbolic curve for a single binding site (solid line). Error bars are to 1 standard deviation. (D) Gel shift assay of SF3b155 NTD binding to different variations of the AV RNA. The assay was done the same as in (B). Lanes 1−7 are AV-f, forward AV RNA. Lanes 8−14 are AV-r, reverse sequence of AV RNA. Lanes 15−21 are AV-ds, double-stranded AV RNA. Lanes 22−28 are AV-d, single-stranded DNA sequence of AV.

ratio of 1.2 (*32*). Therefore, SF3b155 NTD appears to be a monomer that adopts an elongated structure.

CD spectroscopy was used to determine whether the elongated SF3b155 NTD is structured. The negative absorbance of SF3b155 NTD between 220 and 240 nm suggests some α-helical character, but the large negative peak at 203 nm, blue shifted from the characteristic second α-helix peak, indicates that it is primarily unfolded (Figure 1D and ref *33*). In comparison, U2AF65 contains three RRMs and therefore has more secondary and tertiary structure than SF3b155 NTD. Consistent with its structure, the CD spectra of U2AF65 show the characteristic two negative peaks around 220 and 210 nm indicative of α-helical content (Figure 1D). Melting temperature experiments showed that SF3b155 NTD lacks a sharp melting point, providing further evidence that SF3b155 NTD is primarily unstructured (data not shown). Together, the CD spectra and AUC analysis of SF3b155 NTD show that the elongated shape has little organized structure.

RNA Binding Specificity of the SF3b155 NTD. Previous work has shown that SF3b155 can be cross-linked to bases both 5′ and 3′ of the branch point sequence in the purified A-complex (*16*). In yeast, this region of cross-linking to SF3b155 extends into the PyT and downstream exon during in vitro splicing reactions (*34*). However, SF3b155 contains no sequence similarity to any known RNA binding domains. To determine if SF3b155 NTD can bind RNA, we used a gel mobility shift assay to characterize its RNA binding properties. The A-complex cross-linking studies were performed with the 3′ end of the well-characterized AdML intron (*16*). For RNA binding studies we also used the AdML RNA, containing the BPS, the PyT, and the 3′SS (AV RNA, Figure 2). Figure 2B shows that purified, recombinant SF3b155 NTD forms a complex (complex C) with a ^{32}P-labeled AV RNA. The average fraction bound as a function of total SF3b155 NTD concentration was fit to a single binding site model (Figure 2C) that corresponds to a dissociation constant (K_d) of 8 μM. Although the affinity of SF3b155 NTD for RNA is weak compared to other RNA binding proteins, it is possible that this binding is still biologically significant in the context of other RNA binding proteins. SF3b155 is part of the U2 snRNP, which contains many RNA binding proteins that together can strengthen the total association of U2 snRNP to the intron.

We next asked whether the RNA binding activity of SF3b155 exhibits any nucleotide sequence specificity by measuring its affinity for reverse complement single-stranded RNA, double-stranded RNA, and single-stranded DNA with the same sequence as used in Figure 2B. SF3b155 NTD bound all of the RNA substrates with similar affinity but the DNA with lower affinity. The single-stranded and double-stranded RNAs migrate at the same position on the native gel due to the low percentage polyacrylamide (Figure 2D, lanes 1 and 15). However, when these RNAs are run on a higher percentage polyacrylamide, they migrate at different positions on the gel (data not shown). A nonspecific competitor, such as tRNA, is also able to compete with the AV RNA for SF3b155 NTD binding (data not shown), further suggesting that the interaction between SF3b155 NTD and RNA is nonspecific. Finally, SELEX with GST-tagged SF3b155 NTD did not yield RNAs with higher RNA binding affinity compared to the initial pool of RNA (data not shown). Taken together, these data indicate that SF3b155 NTD binds with low affinity and specificity to nucleic acids. This lack of specificity correlates with the facts that introns are highly degenerate in sequence and that SF3b155 is associated with specific RNA binding proteins in vivo.

Formation of a Ternary Complex Containing RNA, SF3b155 NTD, and U2AF65. U2AF65 and SF1 have previously been shown to bind the PyT and BPS in a cooperative manner (*10*). We hypothesized that SF3b155 and U2AF65 might also influence one another's binding to RNA. A ternary complex between U2AF65, SF3b155 NTD, and RNA can be formed as shown by the formation of the more slowly migrating complex with increasing concentrations of SF3b155 NTD (Figure 3A, lanes 13−16, C2 complex). This ternary complex was not observed with U2AF65 plus RNA (lane 9), nor does it form with SF3b155 NTD and RNA (lanes 2−8). Therefore, we conclude that C2 is a ternary complex between U2AF65, SF3b155 NTD, and RNA.

U2AF65 binds to SF3b155 through the third RRM of U2AF65 (*16*). To assay the interaction between U2AF65 and SF3b155, GST-fused SF3b155 bound to glutathione−Uniflow resin was incubated with the U2AF65 construct indicated (Figure 3B). After extensive washing the proteins were denatured off the beads and fractionated on a protein denaturing gel. The resulting Coomassie-stained gel is shown in Figure 3B. As expected, GST−SF3b155 NTD does not pull down a U2AF65 construct lacking RRM3 (ΔRRM3) in the presence of RNA (Figure 3B, lane 6). Interestingly, in the absence of RNA, GST−SF3b155 NTD does pull down ΔRRM3 (Figure 3B, lane 5). This RRM3-independent SF3b155−U2AF65 interaction was not seen by Gozani and colleagues (*16*), possibly because they used a yeast two-hybrid assay, in which U2AF65 would likely be binding to

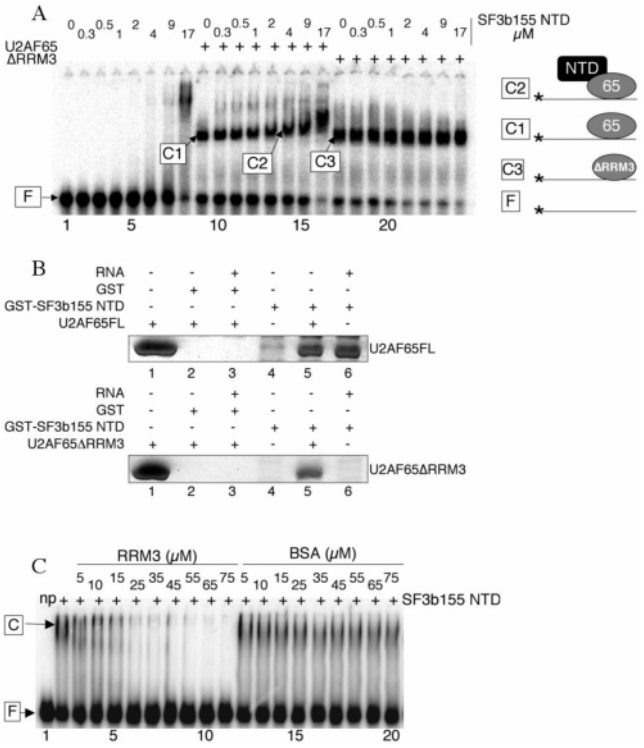

FIGURE 3: RRM3-dependent ternary complex between U2AF65 and SF3b155 NTD on RNA. (A) Gel mobility assay after the binding reaction. Lanes 2−8 are SF3b155 NTD binding AV RNA. Lanes 9−16 are SF3b155 NTD binding AV RNA in the presence of 1 μM U2AF65. Lanes 17−24 are SF3b155 NTD in the presence of 1 μM U2AF65ΔRRM3. np = no protein, and F = free RNA. A schematic of the different complexes is shown to the right of the gel. (B) U2AF65 RRM3 is essential for SF3b155 NTD binding in the presence of RNA. Recombinant U2AF65 constructs were mixed with purified GST-tagged protein in a standard GST pull-down experiment at 125 mM NaCl. SDS−PAGE gels were analyzed by Coomassie stain. Lanes: 1, input U2AF65 full-length (FL) or ΔRRM3, top and bottom gel, respectively; 2, control binding of constructs to glutathione−Sepharose beads with GST; 3 and 4, pull-down of U2AF65/ΔRRM3 with GST−SF3b155 NTD with and without the presence of RNA. (C) RRM3 of U2AF65 competes with RNA for SF3b155 NTD binding. Lanes: 1, AV RNA with no protein; 2, SF3b155 NTD−RNA complex at 10 μM protein; 3−11, constant amount of SF3b155 NTD with increasing concentrations of RRM3; 12−20, same as lanes 3−11 but with increasing concentrations of BSA.

various nuclear yeast RNAs. The binding observed between SF3b155 and ΔRRM3 is possibly due to SF3b155 interacting with either RRM1 or RRM2 on their RNA binding surfaces because the interaction is blocked in the presence of RNA.

To determine whether the interaction between U2AF65 and SF3b155 NTD is required for the formation of a ternary complex, the ΔRRM3 construct was used in place of full-length U2AF65 (Figure 3A, lanes 18−24). ΔRRM3 binds RNA with affinity comparable to full-length U2AF65 (lane 18) but does not form a ternary complex with SF3b155 NTD (lanes 19−24). Also, the presence of ΔRRM3 appears to inhibit SF3b155 NTD binding to RNA, because no additional bands are observed with increasing concentrations of SF3b155 NTD. However, the amount of free RNA does decrease, indicating either more binding by ΔRRM3 or weak binding by SF3b155 NTD, which is not observed as a discrete band on the gel. This result indicates that a ternary complex of U2AF65, SF3b155 NTD, and RNA requires the protein−protein interaction between U2AF65 and SF3b155 NTD and suggests that SF3b155 NTD may not interact directly with RNA when U2AF65 is present.

Next we determined whether SF3b155 NTD bound to RNA could recruit RRM3 of U2AF65 to form a ternary complex. RRM3 of U2AF65 is unable to bind RNA because it contains an extra α-helix that blocks the RNA binding face of the RRM domain (*35*). Therefore, a ternary complex formation on RNA would be completely dependent on SF3b155 NTD binding RNA. Strikingly, not only does a ternary complex not form, but the addition of RRM3 inhibits SF3b155 NTD RNA binding (Figure 3C, lanes 3−11). In contrast, the addition of BSA to SF3b155 NTD RNA binding reaction had only a minimal effect on SF3b155 NTD RNA binding (Figure 3C, lanes 12−20). This result suggests that the RNA and U2AF65 binding sites within SF3b155 NTD overlap.

SF3b155 Contains Multiple U2AF65 Binding Sites. A previous study using the GST pull-down assay and NMR revealed that RRM3 of U2AF65 recognizes a short peptide in the N-terminus of SF1 (*35*). The two most important amino acids for this interaction are an arginine and a neighboring tryptophan (Figure 4A, bottom sequence). Phosphorylation of the serine that is N-terminal to the arginine inhibits this interaction (*36*). Also important, but to a lesser degree, are the N-terminal basic amino acids. Binding is disrupted when all of the basic residues are mutated to acidic residues (*35*). Since SF1 and SF3b155 have both been shown to interact with RRM3 of U2AF65, we sought to identify potential U2AF65−RRM3 binding sites in SF3b155 NTD by aligning the RRM3 binding peptide from SF1 with regions of SF3b155 NTD that contain a tryptophan (Figure 4A). Five SF3b155 peptides were identified that contain the two most important amino acids (Arg and adjacent Trp); these were chosen for binding studies with U2AF65. As previously reported (*16*, *35*), SF3b155 NTD and the SF1 peptide interact with recombinant U2AF65 in a GST pull-down assay (Figure 4B, lanes 2 and 3). All five SF3b155 peptides also pull down U2AF65 (Figure 4B, lanes 5−8), while GST alone did not (lane 9). To determine if there was any difference in binding affinity among the peptides, more stringent conditions were tested. All five SF3b155 peptides were able to bind weakly up to 100 mM NaCl, while 150 mM NaCl inhibited binding for all five peptides and the control SF1 peptide to U2AF65 (data not shown). Therefore, there are at least five sites on SF3b155 NTD that U2AF65 recognizes and binds.

As a further test of the specificity of the interactions between these SF3b155 peptides and U2AF65, we performed a competition assay using a preassembled ternary complex of RNA−U2AF65−SF3b155 NTD (Figure 4C, complex C2). Increasing amounts of GST−peptides A and G were able to disrupt this complex and form a new complex (RNA−U2AF65−GST−peptide, Figure 4C, complex C3). GST−peptides A and G began to form a visible C3 complex at 23 μM (lanes 5 and 17), while GST−peptides C, E, and H formed no C3 complex at 90 μM (lanes 12, 16, and 24). The ability of peptides A and G to compete for binding to U2AF65 in this assay correlates with the fact that these peptides are most similar in sequence to the U2AF65 binding peptide in SF1. Although in the GST pull-down assay differences were not observed among the peptides, the competition assay more closely resembles the in vivo

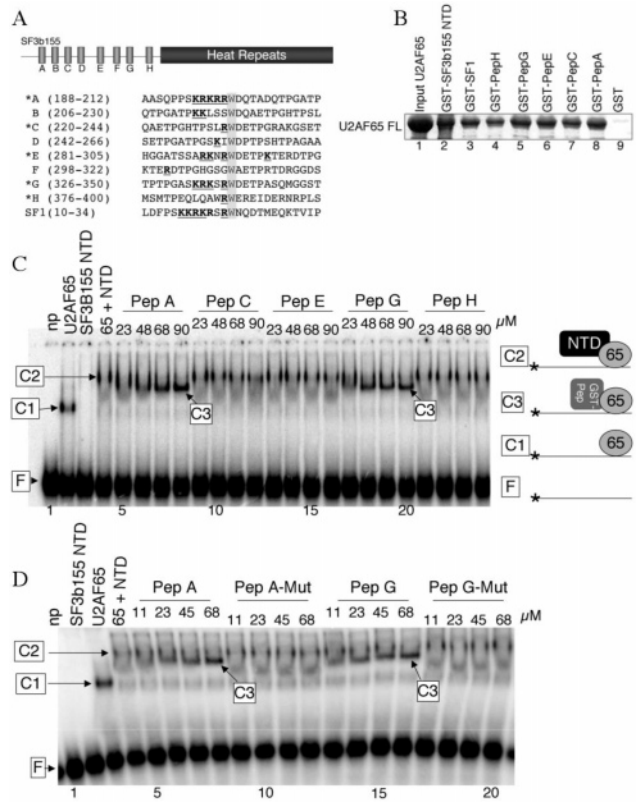

FIGURE 4: SF3b155 NTD contains multiple U2AF65 binding sites. (A) A schematic representation of SF3b155 and alignment of potential U2AF65 binding sites within SF3b155 NTD compared to the U2AF65 binding site with SF1. The lettered squares (A−H) are the eight regions of SF3b155 NTD that contain tryptophans (W, gray box). The positively charged residues upstream of the tryptophan are in bold and underlined. The final peptide in the alignment is an SF1 peptide that binds to RRM3 of U2AF65 (*35*). The starred peptides are those used in this study. (B) GST pull-down assay of U2AF65 at 80 mM NaCl. Lanes: 1, input U2AF65; 2, positive control of GST−SF3b155 NTD; 3−8, GST fusion peptide; 9, negative control of GST alone on glutathione−Sepharose beads. (C) Gel mobility assay after the competition reaction between SF3b155 NTD and the peptides for U2AF65−RNA binding. RNA was prebound with U2AF65 (65, lane 3), SF3b155 NTD (lane 2), or both (65 + NTD, lanes 4−24). Lanes 5−25 were then incubated with the indicated amount of peptide. np = no protein, 65 = 1 μM U2AF65, and NTD = 3 μM SF3b155 NTD. The complexes formed are illustrated to the right of the gel. (D) Peptide mutants are the same as their wild-type sequence except the tryptophan (see sequences in panel A) is mutated to an alanine. The same experimental procedure was used as in panel C.

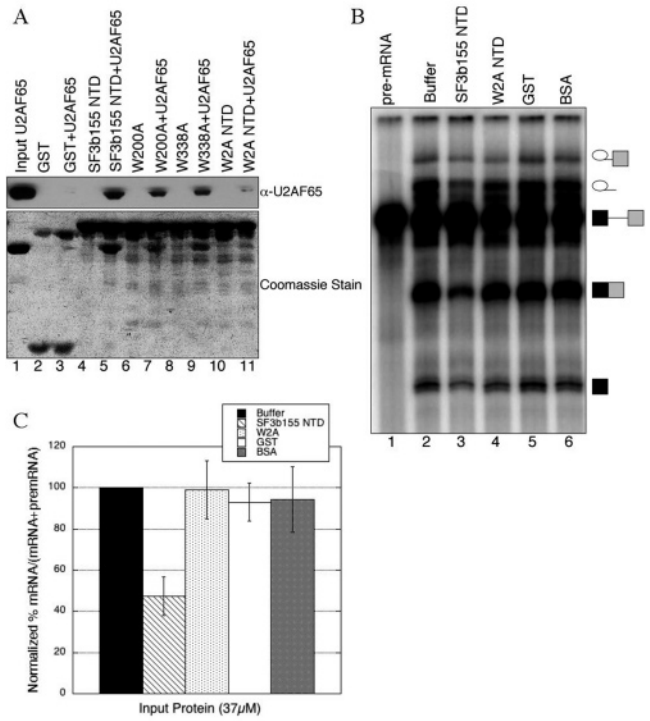

FIGURE 5: Inhibition of splicing by SF3b155 NTD. (A) The double mutant shows a decrease in U2AF65 binding. Lanes: 1, input U2AF65; 2−11, GST fusion proteins incubated with either U2AF65 or dialysis buffer, washed in 125 mM NaCl wash buffer, and then fractionated on a protein denaturing gel. The top analysis was done by Western with a U2AF65 antibody. The bottom analysis was a Coomassie stain of the GST pull-down assay to show equal loading of GST-tagged proteins. (B) SF3bb155 constructs were analyzed for their ability to inhibit splicing of AdML RNA after 2 h of incubation. Total RNA was fractionated on a 15% denaturing polyacrylamide gel. Lanes: 1, input pre-mRNA; 2, splicing in the presence of protein dialysis buffer; 3, addition of 37 μM SF3b155 NTD; 4, addition of 37 μM GST−W2A (SF3b155 NTD W200A, W338A); 5, addition of 37 μM GST; 6, addition of 37 μM BSA. Symbols to the right of the gel represent the lariat intermediate, lariat intron, pre-mRNA, mRNA, and 5′ exon (top to bottom). (C) Quantitation of the percent splicing [% mRNA/(mRNA + pre-mRNA)] over four different gels using a Phosphoimager and shown in the graph. Each individual gel was normalized for wild-type splicing equal to 100% to account for variability in the HeLa extract.

scenario in which U2AF65 is bound to RNA. We have already shown that the presence of RNA can have an effect on the interactions available to U2AF65 (Figure 3B). The competition assay reveals that GST−peptides A and G are better substrates for U2AF65 while GST−peptides C, E, and H are lower affinity sites for U2AF65. Interestingly, peptide G, but not peptide A, contains a serine, which could be phosphorylated in a manner similar to the SF1 binding site (*36*). However, no data have been reported that address whether SF3b155 is phosphorylated by the same kinase as SF1 (cGMP-dependent protein kinase I). The established phosphorylation of SF3b155 by cyclin E−cdk2 maps to sites that do not overlap with the serine in peptide G (*21*).

To assess the importance of the tryptophans in GST−peptides A and G, derivatives of the GST−peptides A and G containing tryptophan to alanine substitutions (Pep A Mut and Pep G Mut) were used in the competition assay. These mutations completely abolished the ability of Pep A Mut and Pep G Mut to disrupt the RNA−U2AF65−SF3b155 NTD complex (Figure 4D, lanes 9−12 and 17−30, respectively), demonstrating that the tryptophan in these peptides is essential for the U2AF65−SF3b155 interaction. Next we wanted to determine if, in the context of the entire NTD, both high-affinity sites were important for U2AF65 binding. First, we looked at single point mutations that changed the tryptophan from peptide A (W200A) or peptide G (W338A) to an alanine. The single point mutations showed only slightly decreased U2AF65 binding (Figure 5A, lane 5 compared to lanes 7 and 9). When both tryptophans are mutated (W2A), binding of U2AF65 is almost completely reduced compared to the wild-type SF3b155 NTD and the single point mutations (lane 11 compared to lanes 5, 7, and 9). This reduction in U2AF65 binding is not due to a difference in the amount of GST-tagged SF3b155 NTD and corresponding mutants (Figure 5A, bottom Coomassie gel). The three weaker U2AF65 binding sites in SF3b155 are

likely not binding to U2AF65 because of the increased salt (150 mM NaCl) used to assay the interaction between U2AF65 and SF3b155 or due to the accessibility of these sites in the context of a full-length SF3b155 NTD.

SF3b155 NTD Inhibits in Vitro Splicing. The NTD of SF3b155 is less conserved than the C-terminal HEAT repeats, suggesting that the NTD may be less important for splicing. To determine if SF3b155 NTD plays a significant role in splicing, we tested the ability of NTD to affect splicing using a trans-inhibition assay similar to that used previously for the splicing factors CDC5L and PLRG1 as well as certain kinases (*37*, *38*). The addition of SF3b155 NTD to HeLa nuclear extract causes a 50% inhibition of splicing compared to the addition of control proteins GST and BSA (Figure 5B, compare lane 3 to lanes 5 and 6), indicating the importance of SF3b155 NTD in splicing. This inhibition of splicing is likely due to SF3b155 NTD binding to U2AF65 and blocking U2 snRNP binding. To test if SF3b155 NTD is inhibiting splicing by blocking U2 snRNP binding to U2AF65, we used the double mutant construct described above (W2A) that showed a significant decrease in the ability to bind U2AF65 (Figure 5A). Addition of SF3b155 W2A did not inhibit splicing (Figure 5B, lane 4), indicating that SF3b155 W2A is no longer capable of sequestering U2AF65 in the extracts and that other regions of SF3b155 are not acting to sequester essential splicing factors at the concentrations tested. These results demonstrate that SF3b155 NTD does play a significant role in splicing and that role is linked to the two high-affinity U2AF65 binding sites in SF3b155.

U2AF65 and p14 Bind Distinct Regions of SF3b155 NTD. It has been shown that another RRM-containing protein, p14 of U2 snRNP, interacts with SF3b155 NTD (*20*). The interaction was mapped to amino acids 255−424 of SF3b155 (*20*). Since p14 is little more than an RRM domain, we predicted that this protein interacts with SF3b155 NTD via its RRM. This was confirmed by showing that the predicted p14 RRM (amino acids 10−95) is sufficient for binding to SF3b155 (Figure 6B, lane 3). We then tested the five SF3b155 NTD GST−peptides, which interact with RRM3 of U2AF65, for interaction with p14. Of these, only peptides E, G, and H lie within the previously mapped interaction region for p14 (*20*). None of the GST−peptides bind p14 in the GST pull-down assay (data not shown). We conclude from this result that either p14's binding site is distinct from those of U2AF65 or that an extended region of SF3b155 is necessary for p14 binding. To define the binding site of p14 on SF3b155, we made several GST fusion constructs of SF3b155 and tested them for binding to p14 in the GST pull-down assay (Figure 6A,C). The smallest construct that binds p14 is SF3b155 (396−424). This region of SF3b155 is highly conserved, even among distantly related organisms (Figure 6D). The amino acids in the p14 binding site are 50% identical between *S. pombe* and *H. sapiens*, while the entire NTD is only 23% identical between these organisms. The only organism, in which the SF3b155 gene has been sequenced, that lacks this conserved region is *Saccharomyces cerevisiae*. This correlates with recent work showing that the proposed p14 yeast orthologue is not a part of the budding yeast SF3b complex (*39*). These results indicate that the highly conserved p14 interaction site on SF3b155 NTD mediates a novel type of RRM−protein interaction that differs from the interaction between U2AF65's RRM3 and

Figure 6

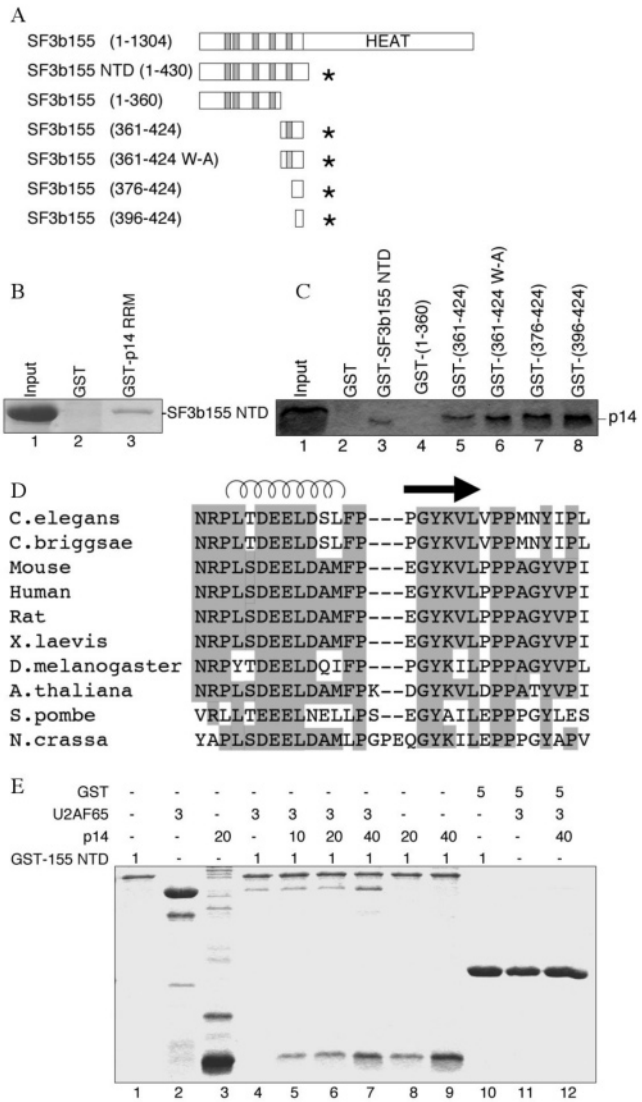

FIGURE 6: SF3b155 binds the RRM of p14 in a tryptophan-independent manner. (A) Primary structure of SF3b155 and schematic representation of the GST-fused fragments of SF3b155 used to determine the region of p14 interaction. The filled boxes represent the five peptides shown to interact with U2AF65 (Figure 5). The hatched box represents the two tryptophans (W386, W388) mutated to alanines. Stars indicate the fragments of SF3b155 that bound to p14. (B) GST pull-down assay of the SF3b155 NTD with GST−p14 RRM at 300 mM NaCl. Lanes: 1, input SF3b155 NTD; 2, control binding to glutathione−Sepharose beads with GST; 3, SF3b155 NTD binding to GST−p14 RRM (amino acids 10−95). (C) GST pull-down assay of p14 with SF3b155 fusion proteins (lanes 4−9) at 300 mM NaCl. Lanes: 1, input p14; 2, control pull-down assay with GST alone on glutathione−Sepharose beads. (D) A multiple sequence alignment of the p14 binding domain (amino acids 396−424) of putative SF3b155 orthologues. Residues identical in at least six of the organisms are highlighted in gray. The positions of the predicted α-helix and β-sheet are indicated above the alignment. (E) Coomassie-stained SDS−PAGE GST pull-down assay of GST−SF3b155 NTD binding U2AF65 in the context of increasing p14 concentrations at 100 mM NaCl. Concentrations of proteins in the reaction are above the lanes. All concentrations are in μM. Lanes: 1, GST−SF3b155 NTD; 2, input U2AF65; 3−7, GST−155 NTD pulling down U2AF65 with increasing p14 concentrations; 8−11, GST−155 NTD pulling down increasing amounts of p14 without U2AF65 present; 12, input p14.

SF3b155 NTD. Further supporting the model that SF3b155 is functioning as a scaffold, we show that not only does

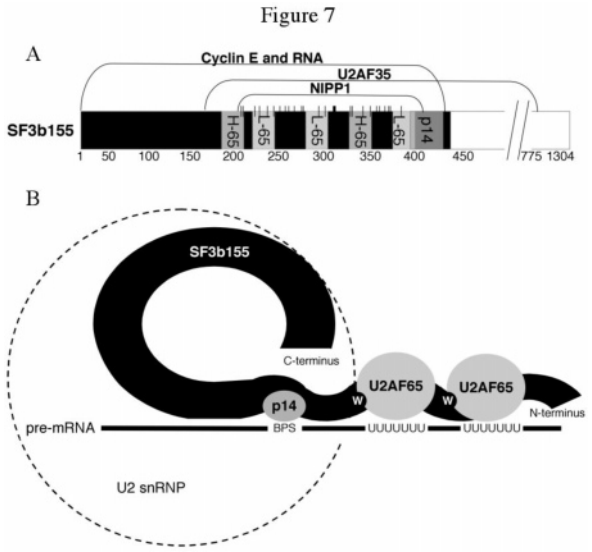

FIGURE 7: Model of SF3b155 NTD as a scaffold. (A) Map of SF3b155 NTD. H-65 means high-affinity U2AF65 site, L-65 means low-affinity U2AF65 site, p14 means p14 binding site. Hatch marks are the phosphorylated TP repeats. The bold hatch mark is the high-affinity binding site for NIPP 1 (*22*). (B) Model of SF3b155 NTD as the tail of U2 snRNP, making interactions that help to recruit and stabilize the U2 snRNP on the intron.

SF3b155 have distinct sites for binding U2AF65 and p14 but an excess of either p14 (Figure 6E) or U2AF65 (data not shown) does not disrupt the ability of GST−155 NTD to pull down the other protein.

DISCUSSION

U2 snRNP plays an important role in preparing the intron to undergo the chemistry of splicing. One of the critical interactions involves base pairing between the BPS and the U2 snRNA, which presents an unpaired adenosine that serves as the nucleophile in the first transesterification reaction (*40*, *41*). Yet many human introns lack a complementary BPS for optimal base pairing to the U2 snRNA. Other mechanisms are, therefore, required for the recruitment and stabilization of the U2 snRNP on the intron. We propose that SF3b155's NTD acts as a tail or scaffold for the binding of many splicing factors, including those involved in U2 snRNP recruitment and stabilization. All known SF3b155 orthologues contain an NTD, although it varies in length and content. We show that human SF3b155 NTD is primarily unfolded and adopts an elongated shape, maximizing its interaction surface for binding many factors simultaneously. Splicing factors U2AF65, p14, NIPP1, and cyclin E have all been shown to bind the NTD [Figure 7A (*16*, *20*−*22*)]. We show that p14 and U2AF65 bind distinct sites on SF3b155 NTD. The binding of U2AF65 or p14 to SF3b155 NTD does not affect the ability of the other protein to bind; an excess of either protein does not inhibit binding of the other protein in a GST pull down (Figure 6E). It will be interesting to determine if other factors shown to bind the NTD, such as cyclin E and Nipp1, can also bind SF3b155 NTD simultaneously.

RNA Binding of SF3b155 NTD. All RNAs tested showed similar binding affinities to SF3b155 NTD and SELEX experiments were not successful in extracting high-affinity binding RNAs. These results suggest that SF3b155 NTD binds RNA nonspecifically. There is precedent for the cooperation between sequence-specific and nonspecific RNA binding proteins or domains. Such is the case in U2AF65's RS domain and the cap binding complex eIF4 (*42*, *43*). The specific RNA binding domain restricts the area to which the nonspecific interaction can take place, and the nonspecific binding helps to stabilize the entire complex (*44*).

The RNA binding of SF3b155 is likely not important for recruitment of U2 snRNP to the intron. Our data show that although SF3b155 NTD can bind RNA on its own, the presence of U2AF65 RRM3 inhibits RNA binding, suggesting that the RW motifs may bind both RNA and protein. This result implies that after U2AF65 leaves the splicing complex, which is thought to occur at the A to B complex transition in splicing, the RNA binding of SF3b155 NTD may help to stabilize U2 snRNP binding on the intron. It will be interesting to determine whether phosphorylation affects the RNA binding of SF3b155 NTD. Phosphorylation would decrease the already low p*I* (5.95) of SF3b155 NTD, potentially inhibiting the RNA binding activity of SF3b155.

The RNA binding observed for the RS domain of U2AF65 as well as SR proteins (*45*−*47*) may serve as a model for SF3b155 NTD RNA binding activity. The RS domains of U2AF65 and SR proteins have been cross-linked to the BPS and 5′ SS, respectively, and are proposed to stabilize weak pre-mRNA−snRNA interactions (*45*−*47*). The RNA binding of SF3b155 NTD could be involved in helping the 3′ end of the intron and associated snRNAs adopt the proper conformation for spliceosome formation and catalysis. Further studies will be necessary to determine the role of SF3b155 NTD RNA binding in spliceosome formation and catalysis.

p14 Binding Site on SF3b155. Previous work showed that p14 and U2AF65 have overlapping binding sites on SF3b155, suggesting that p14 may replace U2AF during spliceosome assembly (*16*, *20*). In contrast to this model, we found that the U2AF65 and p14 binding sites on SF3b155 are distinct from one another. U2AF65 binds a motif that contains an essential tryptophan and is rich in basic amino acids. The p14 binding site (amino acids 396−424) is quite different from the U2AF65 sites. The p14 site does not contain a tryptophan, and the site is acidic rather than basic (Figures 4A and 6D). This region of SF3b155 is predicted to fold into an α-helix followed by a β-strand (Figure 6D), suggesting that the RRM of p14 binds a structured motif. The sequence conservation of this site among SF3b155 orthologues suggests that this region is bound by p14 in all studied eukaryotes except *S. cerevisiae*, in which p14 is not part of the SF3b complex (*39*). Additionally, the location of the p14 binding site is always at the end of the NTD, shortly before the HEAT repeats. This may have implications for the structure and mechanism of p14 binding, in which there is a necessary distance needed between the HEAT repeats and the p14 binding site.

A recent publication by Spadaccini and colleagues validates our results of the p14−SF3b155 interaction (*48*). They too found that p14 binds a small peptide of SF3b155 and that this region of SF3b155 is in an α-helical structure. They found that, unlike other RRM−protein interactions, the SF3b155 interaction surface is on the β-sheet side of the RRM, typically found to be the RNA interaction surface. Furthermore, a recent crystal structure of p14 in complex with a peptide from SF3b155 confirms these results (*49*).

SF3b155 Contains Multiple U2AF65 Binding Sites. The GST pull-down and competition assays show that SF3b155 contains at least five potential U2AF65 binding sites (Figure 7A). Two of these sites bind with higher affinity to U2AF65 than the others, as demonstrated in our competition assay (Figure 4C). Mutating these two high-affinity sites eliminates the ability of SF3b155 NTD to block splicing (Figure 5), indicating that these two sites are the primary sites of interaction for U2AF65 in recruiting U2 snRNP to the BPS. There are several models to explain why SF3b155 contains multiple U2AF65 binding sites. One is shown in Figure 7B; multiple U2AF65 molecules bound to the intron could result in more efficient recruiting of U2 snRNP to the intron compared to when only one U2AF65 molecule is bound to the intron. Multiple U2AF65−SF3b155 interactions could compensate for weak interactions elsewhere, such as a weak U2 snRNA−BPS interaction. Regulating these multiple interactions could be a way to control alternative splicing. For example, modification or masking of one of these SF3b155 sites under certain conditions could result in changes in the splicing pattern of the pre-mRNA. Second, the multiple U2AF65 sites may simply increase binding between SF3b155−U2AF65 by increasing the local concentration of SF3b155. Splicing is not only precise and accurate but efficient as well. The multiple sites may increase the rate at which the A-complex forms on introns. Finally, the multiple U2AF65 sites may not all be bound by U2AF65 in vivo. There are many putative protein-binding RRMs (*50*); any of these may also be interacting at the U2AF65 sites of SF3b155.

Thickman and colleagues also recently found multiple U2AF65 sites in the NTD of SF3b155 (*51*). In their study, they used isothermal calorimetry and fluorescence anisotropy to identify five binding sites and found that SF3b155 is capable of binding three U2AF65 molecules simultaneously. Although we both identified five U2AF65 binding sites in SF3b155, only four are shared. The four sites found in both studies are peptide sites A, C, E, and G. We also found that peptide H was a binding site while they found that peptide B was a site. This suggests there are six binding sites for U2AF65 on SF3b155. Both studies agree that peptide G is a high-affinity site while we differ on the other high-affinity site. Our second high-affinity site is peptide A while their second high-affinity site is peptide E. These differences in high-affinity sites are likely due to the use of different assays.

Comparison of SF3b155 NTD to the C-Terminal Domain of Polymerase II. Several similarities between SF3b155 NTD and the C-terminal domain (CTD) of RNA polymerase II suggest that SF3b155 NTD may be a scaffold in the U2 snRNP particle that has one role in early splicing and a different role in the later stages, much like the CTD of Pol II in transcription (reviewed in ref *52*). Like the Pol II CTD, SF3b155 NTD is an elongated domain shown to associate with multiple factors. In addition, both the CTD and the SF3b155 NTD consist of repeats that increase with the complexity of the organism. Mammalian SF3b155 NTD has 7 RWDETP and 13 TPG repeats, while fission yeast has only 2 RWDETP repeats and no TPG repeats. The CTD consists of heptad repeats: 52 in mammals and 26 in yeast (*53*). Finally, both the CTD and SF3b155 NTD undergo multiple phosphorylation events. These modifications are linked to a change in the activity of the complex: elongation for the Pol II complex and cleavage for the spliceosome (*54*, *55*). Future work will hopefully begin to distinguish whether SF3b155 NTD also plays a role in the complex regulation of splicing as seen for the CTD in transcription. The work presented in this study has begun to demonstrate the importance that SF3b155 NTD plays in splicing and the multitude of interactions that take place on the NTD.

ACKNOWLEDGMENT

We thank Alice Barkan, Ken Prehoda, Bea Darimont, and members of the Berglund laboratory for helpful experimental advice and suggestions on the manuscript. We also thank Robin Reed and Charles Query for plasmids.

REFERENCES

1. Brow, D. A. (2002) *Annu. Rev. Genet. 36*, 333−360.
2. Roscigno, R. F., Weiner, M., and Garcia-Blanco, M. A. (1993) *J. Biol. Chem. 268*, 11222−11229.
3. Reed, R., and Maniatis, T. (1985) *Cell 41*, 95−105.
4. Reed, R. (1989) *Genes Dev. 3*, 2113−2123.
5. Frendewey, D., and Keller, W. (1985) *Cell 42*, 355−367.
6. Garcia-Blanco, M. A., Jamison, S. F., and Sharp, P. A. (1989) *Genes Dev. 3*, 1874−1886.
7. Ruskin, B., and Green, M. R. (1985) *Nature 317*, 732−734.
8. Reed, R. (2000) *Curr. Opin. Cell Biol. 12*, 340−345.
9. Mount, S. M. (1983) *Nature 304*, 309−310.
10. Berglund, J. A., Abovich, N., and Rosbash, M. (1998) *Genes Dev. 12*, 858−867.
11. Zamore, P. D., Patton, J. G., and Green, M. R. (1992) *Nature 355*, 609−614.
12. Wu, S., Romfo, C. M., Nilsen, T. W., and Green, M. R. (1999) *Nature 402*, 832−835.
13. Huang, T., Vilardell, J., and Query, C. C. (2002) *EMBO J. 21*, 5516−5526.
14. Nelson, K. K., and Green, M. R. (1989) *Genes Dev. 3*, 1562−1571.
15. Hodges, P. E., and Beggs, J. D. (1994) *Curr. Biol. 4*, 264−267.
16. Gozani, O., Potashkin, J., and Reed, R. (1998) *Mol. Cell. Biol. 18*, 4752−4760.
17. Brosi, R., Hauri, H. P., and Kramer, A. (1993) *J. Biol. Chem. 268*, 17640−17646.
18. Kramer, A., Gruter, P., Groning, K., and Kastner, B. (1999) *J. Cell Biol. 145*, 1355−1368.
19. Golas, M. M., Sander, B., Will, C. L., Luhrmann, R., and Stark, H. (2003) *Science 300*, 980−984.
20. Will, C. L., Schneider, C., MacMillan, A. M., Katopodis, N. F., Neubauer, G., Wilm, M., Luhrmann, R., and Query, C. C. (2001) *EMBO J. 20*, 4536−4546.
21. Seghezzi, W., Chua, K., Shanahan, F., Gozani, O., Reed, R., and Lees, E. (1998) *Mol. Cell. Biol. 18*, 4526−4536.
22. Boudrez, A., Beullens, M., Waelkens, E., Stalmans, W., and Bollen, M. (2002) *J. Biol. Chem. 277*, 31834−31841.
23. Golas, M. M., Sander, B., Will, C. L., Luhrmann, R., and Stark, H. (2005) *Mol. Cell 17*, 869−883.
24. Wang, C., Chua, K., Seghezzi, W., Lees, E., Gozani, O., and Reed, R. (1998) *Genes Dev. 12*, 1409−1414.
25. Henscheid, K. L., Shin, D. S., Cary, S. C., and Berglund, J. A. (2005) *Biochim. Biophys. Acta 1727*, 197−207.
26. Schuck, P. (2000) *Biophys. J. 78*, 1606−1619.
27. Mayeda, A., and Krainer, A. R. (1999) *Methods Mol. Biol. 118*, 315−321.
28. Corpet, F., Gouzy, J., and Kahn, D. (1998) *Nucleic Acids Res. 26*, 323−326.
29. Rost, B. (1996) *Methods Enzymol. 266*, 525−539.
30. Rost, B., and Sander, C. (1993) *J. Mol. Biol. 232*, 584−599.
31. Wilkins, M. R., Gasteiger, E., Bairoch, A., Sanchez, J. C., Williams, K. L., Appel, R. D., and Hochstrasser, D. F. (1999) *Methods Mol. Biol. 112*, 531−552.
32. Ralston, G. (1993) *Introduction to Analytical Ultracentrifugation*, Vol. 1, Beckman Instruments, Fullerton, CA.
33. Sreerama, N., and Woody, R. W. (2004) *Methods Enzymol. 383*, 318−351.
34. McPheeters, D. S., and Muhlenkamp, P. (2003) *Mol. Cell. Biol. 23*, 4174−4186.

35. Selenko, P., Gregorovic, G., Sprangers, R., Stier, G., Rhani, Z., Kramer, A., and Sattler, M. (2003) *Mol. Cell 11*, 965−976.
36. Wang, X., Bruderer, S., Rafi, Z., Xue, J., Milburn, P. J., Kramer, A., and Robinson, P. J. (1999) *EMBO J. 18*, 4549−4559.
37. Ajuh, P., and Lamond, A. I. (2003) *Nucleic Acids Re.s 31*, 6104−6116.
38. Parker, A. R., and Steitz, J. A. (1997) *RNA 3*, 1301−1312.
39. Dziembowski, A., Ventura, A. P., Rutz, B., Caspary, F., Faux, C., Halgand, F., Laprevote, O., and Seraphin, B. (2004) *EMBO J. 23*, 4847−4856.
40. Berglund, J. A., Rosbash, M., and Schultz, S. C. (2001) *RNA 7*, 682−691.
41. Query, C. C., Moore, M. J., and Sharp, P. A. (1994) *Genes Dev. 8*, 587−597.
42. Forch, P., Merendino, L., Martinez, C., and Valcarcel, J. (2003) *Biochem. J. 372*, 235−240.
43. Magee, J., and Warwicker, J. (2005) *Nucleic Acids Res. 33*, 6694−6699.
44. Singh, R., and Valcarcel, J. (2005) *Na.t Struct. Mol. Biol. 12*, 645−653.
45. Valcarcel, J., Gaur, R. K., Singh, R., and Green, M. R. (1996) *Science 273*, 1706−1709.
46. Shen, H., and Green, M. R. (2004) *Mol. Cell 16*, 363−373.
47. Shen, H., Kan, J. L., and Green, M. R. (2004) *Mol. Cell 13*, 367−376.
48. Spadaccini, R., Reidt, U., Dybkov, O., Will, C., Frank, R., Stier, G., Corsini, L., Wahl, M. C., Luhrmann, R., and Sattler, M. (2006) *RNA 12*, 410−425.
49. Schellenberg, M. J., Edwards, R. A., Ritchie, D. B., Kent, O. A., Golas, M. M., Stark, H., Luhrmann, R., Glover, J. N., and MacMillan, A. M. (2006) *Proc. Natl. Acad. Sci. U.S.A. 103*, 1266−1271.
50. Kielkopf, C. L., Lucke, S., and Green, M. R. (2004) *Genes Dev. 18*, 1513−1526.
51. Thickman, K. R., Swenson, M. C., Kabogo, J. M., Gryczynski, Z., and Kielkopf, C. L. (2006) *J. Mol. Biol. 356*, 664−683.
52. Howe, K. J. (2002) *Biochim. Biophys. Acta 1577*, 308−324.
53. Noble, C. G., Hollingworth, D., Martin, S. R., Ennis-Adeniran, V., Smerdon, S. J., Kelly, G., Taylor, I. A., and Ramos, A. (2005) *Nat. Struct. Mol. Biol. 12*, 144−151.
54. Meinhart, A., Kamenski, T., Hoeppner, S., Baumli, S., and Cramer, P. (2005) *Genes Dev. 19*, 1401−1415.
55. Komarnitsky, P., Cho, E. J., and Buratowski, S. (2000) *Genes Dev. 14*, 2452−2460.

BI060429O